Journal of Colloid and Interface Science 655 (2024) 664–675

Contents lists available at ScienceDirect

Journal of Colloid And Interface Science

journal homepage: www.elsevier.com/locate/jcis

Structure of graphene oxide-phospholipid monolayers: A grazing incidence X-ray diffraction and neutron and X-ray reflectivity study

M. Dolores Merchán [a,b,c], Nisha Pawar [d], Andreas Santamaria [e], Rosalía Sánchez-Fernández [a,e,1], Oleg Konovalov [f], Armando Maestro [d,g,*], M. Mercedes Velázquez [a,b,c,*]

[a] Departamento de Química Física, Facultad de Ciencias Químicas, Universidad de Salamanca, E37008 Salamanca, Spain
[b] Grupo de Nanotecnología, Universidad de Salamanca, E37008 Salamanca, Spain
[c] Laboratorio de Nanoelectrónica and Nanomateriales, USAL-NANOLAB, Universidad de Salamanca, E37008 Salamanca, Spain
[d] Centro de Física de Materiales (CSIC, UPV/EHU) - Materials Physics Center MPC, E-20018 San Sebastián, Spain
[e] Institut Max von Laue and Paul Langevin, 38042 Grenoble, France
[f] European Synchrotron Radiation Facility, 38000 Grenoble, France
[g] IKERBASQUE—Basque Foundation for Science, 48009 Bilbao, Spain

GRAPHICAL ABSTRACT

Cartoons of the mixed monolayers of GO and DPPC and evolution of the volume fraction of each component with the surface pressure.

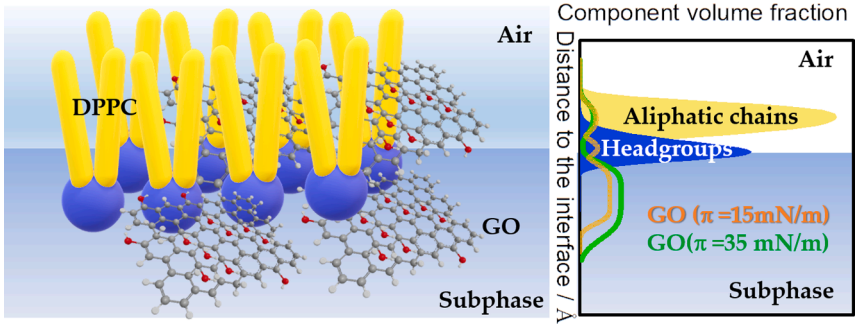

ARTICLE INFO

Keyword:
Graphene oxide
Dipalmitoyl-*sn*-glycerol-3-phosphocholine
Air-water interface

ABSTRACT

Hypothesis: Graphene oxide-based nanotechnology has aroused a great interest due to its applications in the biomedical and optoelectronic fields. The wide use of these materials makes it necessary to study its potential toxicity associated with the inhalation of Graphene Oxide (GO) nanoparticles and its interaction with the lung surfactant. Langmuir monolayers have proven to be an excellent tool for studying the properties of the lung

Abbreviations: f_i^{go}, volume fraction of GO in the i-layers; f_i^{dppc}, volume fraction of DPPC in the i-layer; f_i^{w}, volume fraction of water in the i-layer; t_i, the thickness of the i-layer; σ_i, roughness of the i-layer; ρ_i^{dppc}, SLD value of DPPC into the i-layer; ρ_i^{go}, SLD value of GO into the i-layer; ρ_i^{w}, SLD value of water into the i-layer; ρ_i, SLD value of the i-layer; Φ(z), Volume fraction of a given component of the monolayer, aliphatic chains, head groups or GO, at a distance z from the interface.

* Corresponding author at: Departamento de Química Física, Facultad de Ciencias Químicas, Plaza de los caídos s/n, Universidad de Salamanca, E37008 Salamanca, Spain (M. Velázquez). Centro de Física de Materiales (CSIC, UPV/EHU) - Materials Physics Center MPC, Paseo Manuel de Lardizabal 5, E-20018 San Sebastián, Spain (A. Maestro).
E-mail addresses: armando.maestro@ehu.eus (A. Maestro), mvsal@usal.es (M. Mercedes Velázquez).
[1] Present Address: CICA – Centro Interdisciplinar de Química e Bioloxía y Departamento de Química, Facultade de Ciencias, Universidade da Coruña, E-15071 A Coruña, Spain.

https://doi.org/10.1016/j.jcis.2023.11.022
Received 14 July 2023; Received in revised form 7 October 2023; Accepted 3 November 2023
Available online 10 November 2023

Neutron reflectometry
X-Ray reflectometry
Grazing incident X-ray diffraction

surfactant and the effect of intercalation of nanoparticles on its structure and properties. Therefore, to know the origin of the phospholipids/GO interaction and the structure of the lipid layer with GO, in this work we study the effect of the insertion of GO sheets on a Langmuir film of 1,2-Dipalmitoyl-*sn*-glycerol-3-phosphocholine (DPPC).
Experiments: Surface pressure-area isotherms, Neutron (NR) and X-ray Reflectivity (XRR) and Grazing Incidence X-ray Diffraction (GIXD) measurements of hydrogenated and deuterated DPPC monolayers with and without GO have been carried out.
Findings: The results outline a strong interaction between the GO and the zwitterionic form of DPPC and prove that GO is in three regions of the DPPC monolayer, the aliphatic chains of DPPC, the head groups and water in the subphase. Comparison between results obtained with hydrogenated and deuterated DPPC allows concluding that both, electrostatic attractions, and dispersion forces are responsible of the interaction GO/DPPC. Results also demonstrated that the insertion of GO into the DPPC aliphatic chains does not induce significant changes on unit cell of DPPC.

1. Introduction

Graphene Oxide (GO) is a derivate of graphene synthesized by oxidation of natural graphite or carbon nanofibers. Its structure has been subject to debate due to its strong dependence on the synthesis procedure and the precursors used for oxidation [1,2]. However, there is wide agreement that GO contains carboxylic and ketone groups mainly located at the edges of sheets, while the basal plane is functionalized by epoxy and hydroxyl groups [3,4]. In recent years, it has been demonstrated that oxidation by concentrated acids produces fragments highly oxidized referred as oxidative debris (OD) [5]. They are constituted by mixtures of polyaromatic molecules strongly oxidized and adsorbed on the GO sheets [6] which affect the GO properties such as the water dispersibility, spectroscopic properties, conductivity, catalytic activity or its interfacial properties [7,8]. These fragments can be eliminated by alkaline washing [1,2,6,9].

The existence of O-groups on the basal plane of graphene oxide allows binding nanoparticles, polymers, or different type of molecules that modulate the properties of the hybrid materials according to the needs of each application. Due its excellent properties, GO and its derivatives are used as component of photovoltaic cells [10], conductive electrodes [11] or light emitting diodes [10]. Besides, its strong dispersibility in water allows its use in biomedical applications such as biosensing [12], bioimaging [13] or as a drug delivery vector [14]. Importantly, it has been found that GO sheets adsorb some drug molecules and can be used as drug carriers [15]. Besides, GO-DNA complexes are being considered for gene delivering in cells [16]. In these systems, understanding the origin of the interaction between GO and the lipid membrane becomes crucial for delivering these molecules into the cellular matrix.

The wide use of this material in different applications makes it necessary to study its potential toxicity associated with the inhalation of these particles and its incorporation into the lung surfactant (LS). LS is the first barrier against inhaled pathogens which can alter the composition, or the organization of the lipid membrane, modifying their properties [17]. These changes drive to dysfunctions in the behavior of LS with important effects on the respiratory process [18–20]. GO toxicity studies have been studied in recent years, showing different biological responses depending on the size, shape and concentration of GO sheets and the administration route [21,22]. Concerning its effect on the alveolar cells, it has been shown that the administration of GO in mice develops fibrosis in lung tissues [23]. In addition, it was reported that the retention of GO on the lung surfactant film destroys its structure, modify its biophysical properties resulting potentially toxic [24]. In other situations, it was demonstrated that GO inhalation caused strong inflammatory response by releasing cytokines [22]. To interpret the origin of this varied behavior, it is necessary understand the interaction mechanisms of GO with LS at the alveoli as well as the modification of the structure of the lipid bilayer produced by the insertion of the GO sheets [25]. Because the interactions between GO and LS occurs at the interface between the air and the alveolar layer, the GO/LS interactions should be studied at the interface level. In this sense, Langmuir monolayers have proven to be an excellent tool for studying the properties of the lung surfactant and the effect of incorporating different nanoparticles on its structure and functions [18,26].

The lung surfactant is a complex fluid constituted by lipids and proteins which enveloping the pulmonary alveoli allowing the decrease of the surface tension, stabilizing the lung during respiratory cycles, and preventing alveolar collapse at the end of expiration [27]. The complexity of the lung surfactant makes it necessary to reduce the number of components for understanding the role of each one in the surface properties of the film and to study the interactions between the lung surfactant and nanoparticles. The most widely used models reduce the components to 1,2-Dipalmitoyl-*sn*-glycerol-3-phosphocholine (DPPC) [26,28], since it is the main component of the lung surfactant and responsible for the organization of lipids and the reduction of the surface tension [18].

In vitro study of interactions between DPPC and GO have received great attention in recent years. In this sense, using tensiometry [29] and quartz crystal microbalance with dissipation [30] measurements, it was concluded that electrostatic interactions between negatively charged GO sheets and the head groups of phospholipid molecules mainly govern the lipid-GO interactions. However, experimental results show the existence of other interaction forces as hydrogen bonding, or hydrophobic and van der Waals forces [31–33]. So, Molecular Dynamic calculations (MD) indicated that graphene oxide can be embedded in the lipid tails of a bilayer by strong dispersions interactions [34].

In a recent work, using X-ray reflectometry (XRR) and grazing incident X-ray diffraction (GIXD), the interaction between GO and the zwitterionic form of DPPC deposited on solid substrates containing different wt % of GO was studied [33]. Results show two types of diffraction results, GO-rich micro-domains in which the GO sheets penetrate the hydrocarbon tails of the phospholipid molecules and a GO-poor bilayer like the pristine phospholipid molecules. The effect of phospholipid electric charge on the interactions with GO has also been studied by synchrotron X-ray measurements in multilayers adsorbed on solids [32]. Results revealed that GO sheets are accumulated under the positively charged DPPC groups due to electrostatic attractions, while they are repelled by negatively charged phospholipids and present a weak interaction in the case of the neutral phospholipid (zwitterionic form). Interactions between GO and neutral phospholipids have been studied [29,31,35]. However, while some authors reported attractive interactions between them [29], other studies claim no interactions between GO and the zwitterionic form of DPPC [31,35]. This controversial shows that the origin of the interactions between the lipid membrane and GO is still under debate and requires a greater experimental effort to fully understand it. With this objective in mind, in this work we study the structure of DPPC and GO mixed monolayers using NR, XRR, GIXD and tensiometry measurements. We have selected NR, XRR measurements since are key techniques to obtain information about the out-of-plane molecular structure and composition [36–39], while GIXD is a versatile technique to obtain the in-plane molecular structure and lateral packing of phospholipid monolayers at fluid interfaces [40,41]. Besides, to understand the role of non-electrostatic forces as hydrogen bonds, hydrophobic and van der Waals forces in the lipid-GO

interactions, we compare results obtained using two isotopic phospholipid molecules, chain-hydrogenous 1,2-dipalmitoyl-*sn-glycero*-3-phosphocholine (h-DPPC) and chain-deuterated DPPC (d_{62}-DPPC). We have designed this strategy, since it is well established that some intermolecular interactions such as dispersion or hydrogen bonds are weakened when the hydrogen atoms are replaced by deuterium atoms [42]; therefore, through this modification we hope to confirm not only the existence of these interactions, but also their role in the structure of phospholipid/GO monolayers at the air–water interface.

2. Experimental section

2.1. Sample preparation

GO was synthesized by the Hummeŕs method modified by our group to obtain highly oxidized GO sheets of a few layers [7]. Details of the synthesis are in the Supporting Information. The percentage of O groups attached at the graphene oxide sheets was calculated from X-ray photoelectron spectroscopy (XPS) resulting a C/O atomic ratio of 1.46. The sheet size and the surface electric charge were obtained from DLS and by ζ-potential measurements, respectively. The DLS results show a monomodal distribution function with an apparent hydrodynamic diameter value of 615 ± 8 nm while the ζ-potential value of GO aqueous solutions was – 46 mV. All these structural characteristic of GO sheets agree very well with data previously reported [7].

1,2-dipalmitoyl-*sn-glycero*-3-phosphocholine (h-DPPC) and chain-deuterated DPPC (d_{62}-DPPC) were purchased as powder from Avanti Polar Lipids (purity > 99%, Alabaster, AL, USA). Ultra-pure water used for cleaning and preparing the GO subphase solutions was generated by passing deionized water through a Milli-Q unit from Millipore. The total organic content of ultra-pure water was 4 ppb, its resistivity was 18 μΩ·cm and the surface tension 72.5 mN m^{-1}. D_2O (99.9% of isotopic purity) and the reagents used for GO synthesis, $NaNO_3$ (99%), H_2SO_4 (98% w), $KMnO_4$ (>99%), and H_2O_2 (30% w), were provided by Sigma-Aldrich (St. Louis, MO, USA) and used as received.

2.2. Experimental methods.

The surface pressure (Π) - area per molecule (A) isotherms were recorded using a Langmuir trough (model G1, KIBRON, Helsinki, Finland) with a maximum area of 166.4 cm^2. This trough was also used for NR experiments while an in-house setup described below was used for X-Ray experiments. The trough was carefully cleaned with Decon 90 (Decon Laboratories Ltd, Conway St, UK), absolute ethanol (BioUltra, for molecular biology), purity ≥ 99.8%, Sigma-Aldrich, (St. Louis, MO, USA) and Milli-Q. For the isotherms of pristine DPPC, the trough was filled with Milli-Q water or a mixture 8:92 *v/v* % of D_2O: H_2O, known as air contrast matched water (ACMW). To study the interaction between GO flakes and lipid monolayers, GO sheets were dispersed in D_2O or ACMW to the chosen concentration (0.033 mg/ml). Then, the trough was filled with the GO dispersions and the lipid solution in chloroform (0.1 mg/ml) was spread on the subphase using a Hamilton micrometer syringe with a precision of ± 1 μL. After the chloroform was evaporated for about 20 min, the variation of surface pressure during compression at a barrier speed of 8 $cm^2 \cdot min^{-1}$ was recorded using a paper plate (Whatman CHR1 chromatography paper) connected to an electrobalance. In all the experiments the temperature of the subphase was maintained at 21.0 ± 0.5 °C. A calibrated KSV sensor was used to measure the temperature at the surface.

X-ray photoelectron spectrum of GO powder was measured in a VG Escalab 200R spectrometer from Fisons Instruments (Parkton, MD, USA) using an excitation source of Mg Kα ($h\nu = 1253.6$ eV) radiation and a hemispherical electron analyzer. The spectrum was recorded at 20 eV analyzer pass energy. During data acquisition the residual pressure in the analysis chamber was kept below 4×10^{-7} Pa.

Dynamic light scattering (DLS) and ζ-potential measurements were performed on a Zetasizer Nano ZS device (Malvern Instruments, Malvern, UK) at 20.0 °C. In the DLS experiments, the intensity autocorrelation functions were transformed in electric field autocorrelation functions from the Siegert equation. The experimental data sets were obtained at 13°. For ζ-potential experiments, we measured the electrophoretic mobility using a DTS 1060C disposable cell. The electrophoretic mobility values, μ_e, were converted in ζ-potential using the Smoluchowski [43] relationship, $\zeta = \eta\ \mu_e/\varepsilon$, where η and ε are the absolute viscosity and permittivity of water at 20 °C, respectively.

2.2.1. Neutron reflectometry experiments

Specular NR experiments were performed on FIGARO, a time-of-flight reflectometer [44,45] at the Institut Laue-Langevin, (Grenoble, France), using two different angles of incidence ($\theta_1 = 0.6°$ and $\theta_2 = 3.7°$). A wavelength resolution of 7% $d\lambda/\lambda$ was used, yielding a momentum transfer of 0.01 $Å^{-1} < q_z < 0.25\ Å^{-1}$, normal to the interface, and defined as $q_z = (4\pi/\lambda)\sin\theta$, where λ (from 3 to 13 Å) is the wavelength of the neutron beam. In a typical experiment, Reflectivity (*R*), defined as the ratio of the intensity of the neutrons scattered from the air/water interface over the intensity of the incident neutron beam, is measured in specular conditions (i.e., the incident angle of the neutron beam is equal to the reflected angle, denoted as θ) as a function of q_z. The raw time-of-flight experimental data at the two angles of incidence were calibrated with respect to the incident wavelength distribution and the efficiency of the detector yielding the resulting $R(q_z)$ profile using COSMOS [46]. This profile is linked to an in-plane averaged scattering length density (SLD) distribution perpendicular to the interface, which is a measure of the coherent scattering cross-section of the molecular species that constitutes each interfacial layer.

NR data modeling was designed by minimizing the differences between the calculated and the experimental reflectivity profiles. *Aurore* [47] and *refnx* [48] software were used for the data analysis. To minimize the ambiguity of data modeling, the SLD contrast variation method was used for determining the roughness, thickness, and hydration degree of each layer. Therefore, NR experiments were performed using different isotopic subphases for providing distinct contrasts with neutrons, namely 100 % D_2O, a mixture 8:92 *v/v* % of D_2O:H_2O, known as air contrast matched water (ACMW), since its scattering length density is matched to the air at zero and a mixture of 95% h-DPPC and 5% d_{62}-DPPC, referred as contrast matched DPPC, cm-DPPC, because de SLD of the aliphatic tails is zero. To obtain the best set of parameter for each layer the analysis fits simultaneously the reflectivity data measured in the selected contrasts [7].

2.2.2. X-ray scattering experiments

X-ray scattering experiments, specular X-ray reflectometry and grazing incidence X-ray diffraction, were carried out at the ID10 beamline at the European Synchrotron Radiation Facility (ESRF), (Grenoble, France), with X-ray energy of 22 keV and a beam size of 25 × 13 μm^2. Both techniques, XRR and GIXD are extensively described elsewhere [41,49]. Here, an in-house, setup consisting in a PTFE Langmuir trough equipped with a single moveable barrier, was used for both GIXD and XRR experiments. The experiments were performed at two selected surface pressures (15 and 35 mN/m) and at a constant subphase temperature of 21.0 ± 0.5 °C. To minimize the background scattering, the trough was isolated in a Kapton box, and the inside atmosphere was saturated in He (oxygen level < 0.2 %). Different areas of the trough were exposed to the X-rays beam in each particular experiment to avoid radiation damage to the sample [41].

In the case of XRR experiments, *R* was defined as the ratio of the intensity of the X-rays scattered from the air/water interface over the intensity of the incident beam, also measured in specular conditions as a function of q_z, with $\lambda = 1.55$ Å. X-ray scattering density profiles along the direction normal to the interface, similarly to NR, can be extracted [50,51]. XRR data reduction were done using in-house scripts developed at ESRF ID10 and data analysis were done using *refnx* software [48].

For the GIXD experiments, Langmuir monolayers were irradiated with 8 keV X-ray beam energy and at an incidence angle of $\theta = 0.1233°$, 80% below the critical angle of pure water. GIXD 2D contour profiles of the scattered intensity were acquired using a double linear detector (Mythen 2 K) mounted behind a vertically oriented Sollers collimator with an in-plane angular resolution of 1.4 mrad. Diffracted intensities were detected as a function of X-ray momentum transfer component perpendicular, q_z, and parallel to the air/water interface, $q_{xy} = (4\pi/\lambda)\sin 2\theta_{xy}/2$, which further gives the repeat distance $d = 2\pi/q_{xy}$, where $2\theta_{xy}$ is the angle between the incident and diffracted beam projected on the air/water interface. The in-plane component reports the lateral crystalline order in the acyl chains of the phospholipid molecules, whereas the out-of-plane component is used to determine the acyl chain tilting angle and coherence length.

GIXD peaks were obtained by the integration of the 2D profiles along q_z to obtain the so-called Bragg peaks using in-house scripts developed at ESRF ID10. These data were fitted using Voigt functions to obtain unit cell parameters. The in-plane coherence length (L_{xy}) along the crystallographic direction was determined using the Scherrer formula: $L_{xy} = (0.9 \times 2\pi)/FWHM_{xy}$, where $FWHM_{xy}$ is the full width half maxima calculated from the Voigt fitting of the q_{xy} spectrum, respectively.

2.3. Monolayer models used for analyzing XRR and NR profiles

NR and XRR data modelling were performed by minimizing the difference between the experimental data points and the calculated reflectivity profile. The latter was obtained by a model consisting of different layers of constant SLD using Parratt's recursive method [52] with an error function connecting adjacent layers. In the case of DPPC lipid monolayers deposited in pure water, the reflectivity profile was interpreted using a two-layers model that can be rationalized by dividing DPPC molecules between the polar head groups region, in contact with the aqueous subphase, and the aliphatic tails facing the air phase with different SLD values. Molecular volumes of the lipid head groups (V_{heads}) and tails (V_{tails}) and the total neutron and X-ray scattering length of head groups and tails were fixed parameters in the fitting procedure; the values are collected in **Table S1**. The SLD of the layer containing the head-groups is re-parametrized as $\rho_{heads} = f^{w}_{head}\rho^{w}_{heads} + f^{dppc}_{head}\rho^{dppc}_{heads}$, where f^{w}_{heads} is the volume fraction occupied by the water molecules with NR or XRR SLD values referred as ρ^{w}_{heads}, and f^{dppc}_{heads} is the volume fraction of the DPPC head-groups characterized by and SLD referred as ρ^{dppc}_{heads} (**Table S1**). The water volume fraction of the head groups-layer (f^{w}_{heads}) was constrained to ensure the same area per molecule of aliphatic tails (A_{tails}) and head groups (A_{heads}) of the DPPC molecules [53].

In presence of GO, the monolayer was modeled using a three-layers model, the aliphatic chains, the head group and a third layer referred as 3L which only contains GO surrounded by water molecules. We consider that the aliphatic chains and the head group layers incorporate GO sheets, therefore, the SLD values for tails, ρ_{tails}, and for head groups, ρ_{heads} regions are expressed as follows:

$$\rho_{tails} = f^{dppc}_{tails}\rho^{dppc}_{tails} + f^{go}_{tails}\rho^{go}_{tails}$$

$$\rho_{heads} = f^{w}_{head}\rho^{w}_{heads} + f^{dppc}_{head}\rho^{dppc}_{heads} + f^{go}_{head}\rho^{go}_{heads}$$

The SLD of the 3L layer is calculated as:

$$\rho_{3L} = f^{w}_{3L}\rho^{w}_{3L} + f^{go}_{3L}\rho^{go}_{3L}$$

In these equations, f^{go}_{i}, f^{w}_{i} and f^{dppc}_{i} represent the volume fractions of GO sheets, water and DPPC for each i-layer, aliphatic tails, head groups and 3L. Finally, the variation of the volume fraction, $\Phi(z)$, for each component with the distance to the interface, z, was calculated using the model composed of N-layers of varying volume fraction (f_i) and thickness (t_i) modulated by a roughness parameter (σ_i) which describes the interfacial mixing of the layers, as follows:

$$\Phi(z) = \sum_{i=0}^{N} \frac{f_i - f_{i-1}}{2}\left(1 + erf\left(\frac{z - t_i}{\sigma_i\sqrt{2}}\right)\right) \quad (1)$$

3. Results and discussion

3.1. Phospholipid Langmuir films

To study the surface activity and phase behavior of the phospholipid monolayers at the air–water interface, we have recorded the surface pressure-area isotherms of h-DPPC and d_{62}-DPPC on ultrapure water and on aqueous GO solutions (0.033 mg/ml), prior the X-rays and neutron scattering measurements, Fig. 1 **a,c,e**. Since it is expected that the interactions between DPPC and GO modify the mechanical properties of the phospholipid monolayer, the surface compression elastic modulus value, C_s^{-1}, was calculated from the surface pressure isotherms and Eq. (2):

$$C_s^{-1} = -A\left(\frac{d\pi}{dA}\right)_{p,T} \quad (2)$$

where π and A represent the surface pressure and molecular area, respectively. The values are plotted against the surface pressure in Fig. 1 **b,d,f**.

Fig. 1**a** shows the pressure-area isotherms of h-DPPC and d_{62}-DPPC deposited on pure water surface. Results show that the main difference between the isotherms is the LE-LC coexistence region. This region is marked by a plateau in the surface pressure isotherms and a minimum in the compression modulus curves, Fig. 1**b**. The coexistence starts at 3.7 mN/m and 7.8 mN/m for h-DPPC and d_{62}-DPPC, respectively. These values are in excellent agreement with data previously published [53]. Besides, the differences observed between the isotherms of deuterated and hydrogenous phospholipid have been previously reported for other phospholipid monolayers [41] and were attributed to a decrease on the intermolecular attractions between deuterated phospholipid chains relative to the hydrogenous ones [42,53]. Further compression drives to highly condensed monolayers, as revealed by the maximum value of the compression modulus, 290 mN/m. However, in these condensed regions the isotherms of both, the hydrogenated and deuterated phospholipids are quite similar.

As can be seen in Fig. 1**c**, the pressure-area isotherm of h-DPPC spread on GO is more expanded than the isotherm on pure water, while the compression modulus decreases significantly, Fig. 1**d**. These results point to the strong interactions between GO and DPPC probably due to the partition of GO sheets into the lipid monolayer, including the aliphatic chains region, and/or the interaction between the cationic groups of DPPC heads and the negatively charged graphene oxide.

In monolayers of the deuterated phospholipid, the d_{62}-DPPC/GO isotherm is also more expanded than the d_{62}-DPPC one, Fig. 1**e,** and the compression modulus values also decrease compared with the values of pristine d_{62}-DPPC, Fig. 1**f**. However, the effect is less marked than in the isotherm of h-DPPC indicating a weaker interaction in the case of the deuterated chains. To interpret the origin of this behavior, the structure and organization of hydrogenated and deuterated DPPC monolayers with and without GO, have been studied using specular XRR and NR measurements.

3.2. Out-of-plane structure of DPPC thin films studied by X-ray and neutron reflectivity measurements.

We perform XRR and NR measurements to study the out-of-plane structure of monolayers of hydrogenous and deuterated DPPC deposited on pure water and on GO aqueous subphase (0.033 mg/mL). It was necessary to select the surface pressure values using the information

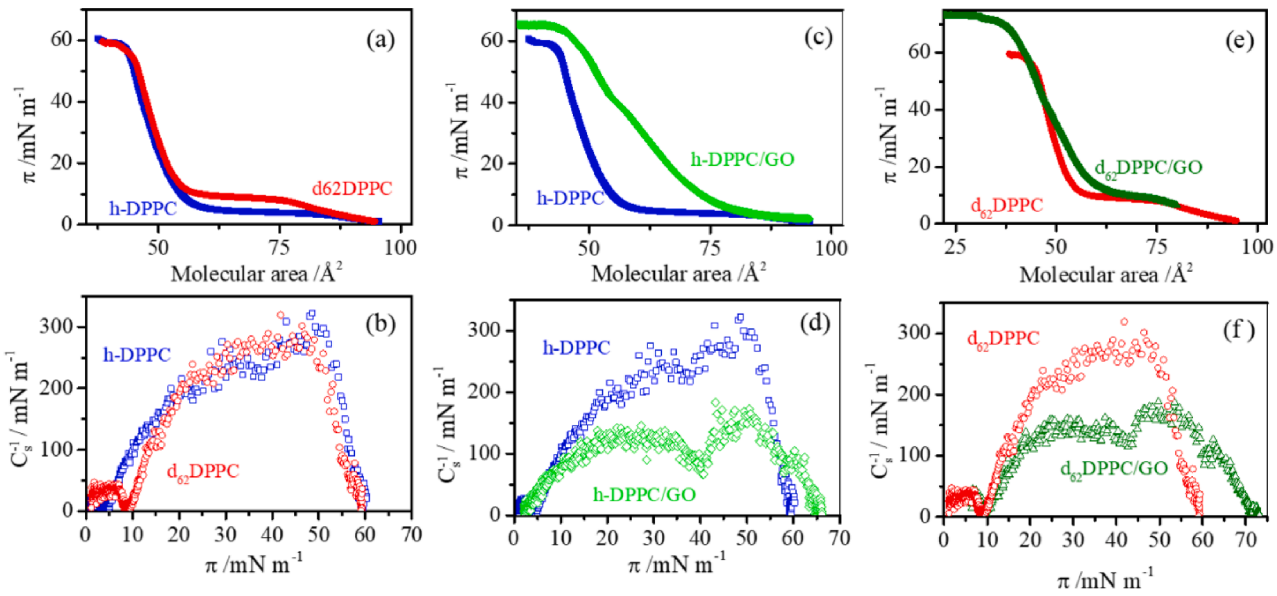

Fig. 1. Surface pressure-area isotherms of: (a) h-DPPC and d_{62}DPPC on pure water; (c) h-DPPC on pure water and 0.033 mg/mL aqueous GO subphase and (e) d_{62}-DPPC on pure water and 0.033 mg/mL aqueous GO solution. Surface compression elasticity modulus of (b) h-DPPC and d_{62}DPPC on pure water, (d) h-DPPC on pure water and 0.033 mg/mL aqueous GO subphase, and (f) d_{62}-DPPC on pure water and 0.033 mg/mL aqueous GO solution. All isotherms were recorded at 21 °C.

taken from the isotherms. Accordingly, it is very beneficial to select systems at a surface pressure in which the monolayers of the two isotopes were in similar phases. For this reason, we have avoided the LE-LC coexistence region, since in that region the structure seems to be quite different for the two isotopic species. Using this criterion, the two surface pressures selected were 15 and 35 mN/m in which the DPPC monolayers are in a condensed state. As can be seen in the isotherms, Fig. 1**a**, at these surface pressure values the two monolayers on water are rather similar, allowing to fit the experimental data jointly. For comparative purposes, we work at the same surface pressure values in phospholipid/GO mixed monolayers.

Initially, the out-of-plane structures of hydrogenated and deuterated DPPC monolayers were resolved by NR and XRR. As was commented, to minimize the ambiguity of data modeling, in the case of NR experiments we have used the following contrasts: ACMW for h-DPPC and d_{62}-DPPC and cm-DPPC on ACMW. In the case of XRR measurements, we used ultrapure water as subphase.

Since these phospholipid molecules yielded laterally homogeneous interfaces on the length scale of the in-plane neutron (and X-rays) coherence length [37], the measured reflectivity curves can be correlated with an averaged SLD depth profile across the interface delimited by this coherence length. To obtain a single set of structural parameters, the calculation was performed by the simultaneous fitting of XRR and NR data of the two monolayers at each surface pressure values and using the molecular volumes and SLD values previously reported [54] and summarized in **Table S1** of the Supporting Information. The experimental results obtained by XRR and NR fit very well the two-layers model, as can be seen in **Fig. S1 a,c,e** of the Supporting Information. This means that the model of the two layers interprets properly the structure of this monolayer. This is in agreement with the results found in the literature [53]. The structural parameters obtained from fits, the thickness (t_i), and the roughness (σ_i) of each i-layer, and the fraction of water molecules associated to each layer, (f_i^w), are collected in Table 1. For comparison Table 1 collects the structural parameters obtained for h-DPPC and d_{62}-DPPC films with GO. The water volume values were calculated by assuming the area per molecule of the acyl chains of DPPC are equal to the area of the DPPC head groups [53]. The averaged SLD depth profiles across the interface are plotted in **Fig. S1 b,d,f** of the Supporting Information.

From the structural parameter collected in Table 1 is possible to

Table 1
Structural parameters obtained from the fitting of XRR and NR profiles to a two-layers model for h-DPPC and d_{62}-DPPC Langmuir monolayers spread out at the air–water interface and from the fits of XRR and NR Reflectivity Profiles to a three-layer model for h-DPPC/GO films and of NR Reflectivity Profiles for d_{62}-DPPC/GO films[a].

Monolayer	Parameter/ units	Acyl chainlayer	Head groupslayer	Aqueous GO (3L)
DPPC (15 mN/m)	t_i / Å	14 ± 1	8 ± 1	–
	f_i^w / %	0	26 ± 2	–
	σ_i/ Å	3 ± 1	3 ± 1	–
	A / Å^2	54 ± 1		–
DPPC (35 mN/m)	t_i / Å	15 ± 1	8 ± 1	–
	f_i^w / %	0	16 ± 1	–
	σ_i/ Å	3 ± 1	3 ± 1	–
	A / Å	48 ± 1		–
h-DPPC (15 mN/m) + GO (0.033 g/L)	t_i / Å	16 ± 1	8 ± 1	31 ± 1
	SLD* / 10^{-6} Å^{-2}	9.62 / 1.06	14.2/ 1.99	9.79 / 0.25
	f_i^w / %	0	14 ± 1	95 ± 2
	f_i^{go} / %	28 ± 2	12 ± 1	5 ± 1
	σ_i/ Å	4 ± 1	6 ± 1	4 ± 1
h-DPPC (35 mN/m) + GO (0.033 g/L)	t_i / Å	17 ± 1	8 ± 1	32 ± 2
	SLD* / 10^{-6} Å^{-2}	10.3/ 0.57	13.98/ 2.56	10.09/ 0.50
	f_i^w / %	0	14 ± 1	90 ± 2
	f_i^{go} / %	19 ± 1	22 ± 1	10 ± 1
	σ_i/ Å	5 ± 1	5 ± 1	4 ± 1
d_{62}-DPPC (15 mN/m) + GO (0.033 mg/ml)	t_i / Å	15 ± 1	8 ± 1	32 ± 1
	SLD** / 10^{-6} Å^{-2}	5.06/7.28	1.89 / 2.71	0.55 ± 0.05
	f_i^w / %	0	3 ± 1	89 ± 3
	f_i^{go} / %	6 ± 1	2 ± 1	11 ± 1
	σ_i/ Å	3 ± 1	3 ± 1	4 ± 1
d_{62}-DPPC (35 mN/m) + GO (0.033 mg/ml)	t_i / Å	17 ± 1	8 ± 1	39 ± 1
	SLD** / 10^{-6} Å^{-2}	6.46/7.34	1.89 / 2.02	0.55 ± 0.05
	f_i^w / %	0	3 ± 1	89 ± 3
	f_i^{go} / %	5 ± 1	2 ± 1	15 ± 2
	σ_i/ Å	4 ± 1	5 ± 1	4 ± 1

* Contrast: XRR / NR.
** Contrast: ACMW / D_2O.
[a] Errors are reported as absolute values calculated in 1σ interval.

conclude that the thickness of the aliphatic tails slightly depends on the surface pressure. The values found in the work are consistent with the molecular dimension of the acyl chain [50]. The thickness of the head group is found independent of the surface pressure and the value agrees very well with that previously reported [53]. In addition, the resultant mean area per molecule values were 54 $Å^2$ (at 15 mN/m) and 48 $Å^2$ (35 mN/m) and are consistent with the values determined from the π-A isotherm. Finally, the values of roughness of each layer (σ_i) obtained from fits are compatible with that corresponding to the theoretical value expected for thermally excited capillary waves [53], ~ 3 Å, and did not significantly vary at the two surface pressures studied.

Fig. 2 shows the out-of-plane structure of the lipid monolayers for the two surface pressure values, reported in terms of the variation of the volume fraction of the acyl chain and head group with the distance to the air–water interface, *z*. The volume fraction was calculated from Eq.1 and the structural parameters listed in Table 1.

Results in Fig. 2**,** show that the area fraction of both the acyl chains and head groups increase after the monolayer compression. Besides, the water fraction of the solvated head groups decreases from 26 % to 16 % as the surface pressure increases, see Table 1. Since the monolayer packing increases as the surface pressure, these facts indicate that the water molecules are squeezed out when the monolayer packing increases due to the barrier compression.

3.3. Effect of GO on the out-of-plane structure of DPPC thin films studied by X-ray and neutron reflectivity measurements.

Interestingly, the interaction between GO and hydrogenated and deuterated chains of DPPC molecules is clearly different looking at the isotherms plotted in Fig. 1**c, e**. To understand the origin of these differences, we studied separately the interactions of GO with h-DPPC and d_{62}-DPPC. The contrasts used were ultrapure water for XRR experiments and ACMW for NR measurements. To minimize the ambiguity of data modeling, XRR and NR profiles were fitted using the same set of parameters, collected in Table 1.

Firstly, the interaction between GO and h-DPPC is addressed. The X-ray and NR reflectivity profiles of h-DPPC/GO monolayers are plotted in Fig. 3**a**.

Conversely to the reflectivity profiles of pristine h-DPPC, the best fits of XRR and NR the reflectivity profiles were obtained from a three-layer model, as shown in Fig. 3 **a**. The model considers a first layer of the aliphatic chains facing the air, an intermediate layer containing the lipid head groups and a third layer facing the bulk, exclusively occupied by GO without traces of lipids, since when lipids were included in the third layer give rise to a worst analysis in terms of the χ^2 value. Simulated curves in Fig. 3**a** were calculated according to the three-layer model and the parameters collected in Table 1. The SLD value for GO in Table 1 was taken from ref. [7].

Parameters in Table 1 show that the structure of monolayers at 15 and 35 mN/m are remarkably different. So, while the fraction of GO in the aliphatic layer decreases from 28 % to 19 % when the pressure increases, the fractions of GO flakes associated to the phospholipid head groups and to the 3rd layer, GO surrounded by water, increase from 12 to 22 % and from 5 to 10%, respectively. This means that, when the surface pressure increases, some GO sheets are displaced from the aliphatic chains of the lipid layer to both, the head group of phospholipids and to the GO aqueous layers. No lipid loss was observed in any of the monolayers studied.

The presence of GO in the head group region can be due to electrostatic attractions between the positively charged choline groups of the phospholipid molecules and the negatively charged carboxylic groups of GO sheets, while the insertion of GO into the aliphatic chains of the phospholipid can be due to non-electrostatic forces, such as dispersions forces which dominate the CH/π interactions [55,56] between the aliphatic chains of lipids and the aromatic network of graphene oxide.

Structural parameters in Table 1 also show that the insertion of GO does not change the thickness of the three layers, the acyl chains, the head group and either the aqueous GO region, while slightly increases their roughness.

It is interesting to consider that, in a previous work, we have studied the structure of monolayers of GO at the air–water interface [7] and we demonstrated that the GO films are constituted of a bilayer formed by a GO layer in contact with air of thickness around 20 Å, and a second layer corresponding to oxidative debris of 10 Å thickness submerged in the aqueous subphase. Therefore, we have included in the model the oxidative debris as a fourth layer, but no better fits were obtained in terms of the improvement of the χ^2 value. However, if we compare the thickness of the GO surrounded by water in the third layer obtained in our fits (31 Å) with the values previously obtained for the GO bilayer, we clearly observe that the thickness obtained in the current work corresponds to the sum of the thicknesses of the two layers, GO and the oxidative debris. Therefore, we conclude that the GO layer below the lipid head groups can be constituted by GO and oxidative debris layers, although it was not possible to separate the contribution of the oxidative debris as an independent layer by fitting our XRR and NR reflectivity profiles. No aggregations between the GO sheets at the interface were detected. This fact agrees with data previously obtained for Langmuir films of non-stacked GO sheets at the air–water interface [7].

The SLD values corresponding to the fits performed to the XRR and NR profiles for films at 15 and 35 mN/m are plotted in Fig. 3 **b.** The

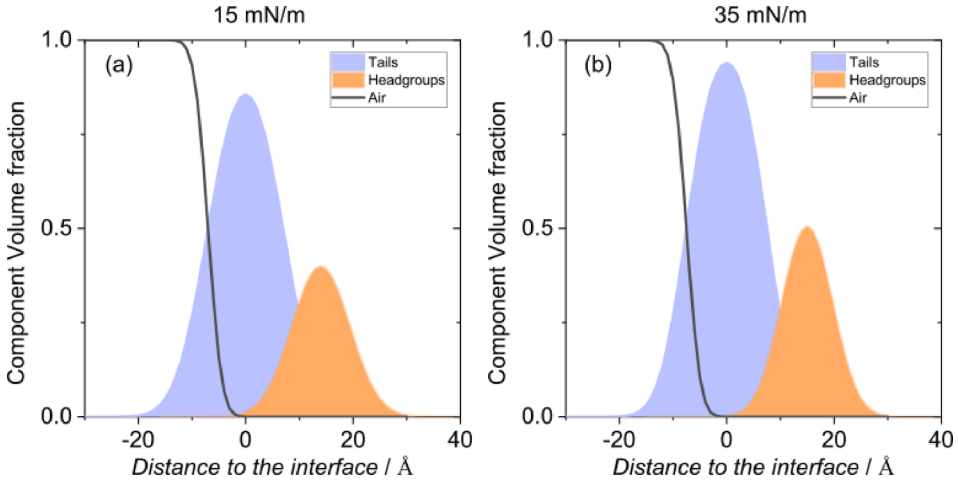

Fig. 2. Volume fraction profiles in the direction normal to the air/water interface of the acyl tails and head groups for DPPC monolayers at 15 mN/m (a) and 35 mN/m (b).

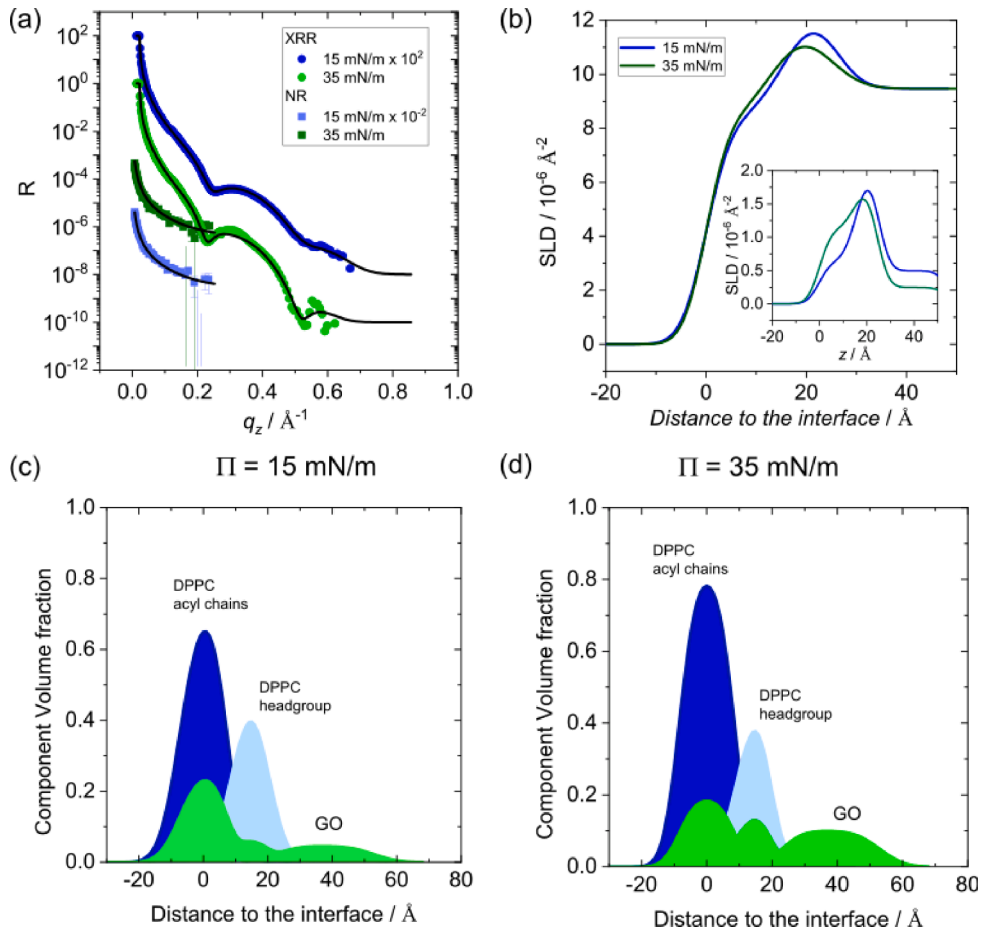

Fig. 3. X-ray and Neutron Reflectometry experimental data for h-DPPC monolayers in the presence of GO dispersed in the subphase: (a) Experimental (symbols) and fits (lines) profiles are plotted versus q_z at the surface pressure values of 15 mN/m and 35 mN/m. From clarity, the profiles corresponding to the surface pressure of 15 mN/m were vertically shifted. (b) SLD profiles across the interface from the XRR measurements. Inset show NR SLD profiles. Variation of the volume fractions with the distance normal to the air/water interface for the different components of monolayers at 15 (c) and 35 (d) mN/m.

variation of the volume fractions of the different components with the distance to the interface, calculated from Eq. (1), and the parameters in Table 1 was plotted in Fig. 3 **c, d.** As can be seen in Fig. 3 **c, d**, the volume fraction of GO sheets intercalated in the aliphatic chains decreases when the surface pressure increases, while it increases in both, the head group, and the aqueous GO regions. This means that the GO sheets are displaced from the acyl chain layer to the head groups and to the aqueous subphase when the monolayer packing increases, i.e., higher surface pressure values.

3.4. Effect of GO on the out-of-plane structure of d_{62}DPPC thin films studied by neutron reflectivity measurements.

To understand the origin of the interactions between GO and DPPC, we have replaced the hydrocarbon chains of h-DPPC by deuterated chains, d_{62}-DPPC and then, NR profiles were recorded. Two isotopic contrast data sets were measured and analyzed together at the surface pressure values of 15 and 35 mN/m. The contrasts were D_2O and ACMW, for both pressures. The corresponding NR reflectivity profiles are reported in Fig. 4 **a, b**.

To model the monolayers of deuterated phospholipid we have also used the three layers model. Fig. 4**c,d** collects the SLD profiles obtained from the analysis of the reflectivity profiles. Finally, in Fig. 4**e,f** the variation of the volume fraction of each component with the distance to the interface for monolayers at 15 and 35 mN/m, are plotted. As in the case of h-DPPC monolayers, the volume fraction values were calculated from Eq. (1) and the parameters in Table 1. The structural parameters in Table 1 were obtained from the best fits of the NR profiles.

The comparison between the parameters obtained from fits for h-DPPC/GO and d_{62}-DPPC/GO, Table 1**,** clearly show that the fraction of GO in the lipid chains is significantly lower for the monolayers of the deuterated chain than for the hydrogenated one. A similar behavior was observed in the layer of the head groups, in which the fraction of GO decreases from 12% (h-DPPC) to 2% (d_{62}-DPPC) for monolayers at 15 mN/m and from 22% (h-DPPC) to 2% (d_{62}-DPPC) for monolayers at 35 mN/m. Conversely, the fraction of GO in the third layer increases from 5 to 10% for monolayers at 15 mN/m and from 10 to 15% for monolayers at 35 mN/m. The variation of the volume fractions of the different components with the distance to the interface are plotted in Fig. 4 **e, f.** Taking together all these results, we can conclude that, conversely to the behavior observed for hydrogenated DPPC monolayers, in d_{62}-DPPC/GO monolayers, the highest percentage of GO sheets is in the region containing GO surrounded by water. Besides, the volume fraction of GO incorporated into the deuterated acyl chains is much lower than that inserted in the hydrogenated chains. All these results indicate a lower penetration of the GO sheets in the region of the deuterated chains than in the hydrogenated as consequence of a weaker interaction between the graphenic network of GO and the deuterated lipid chains. This behavior is consistent with the existence of aryl CH–π interactions [55–57], since these interactions are dominated by dispersion forces [55] which become weaker when hydrogen atoms are replaced by deuterium [58].

We also analyze the effect of packing on the structure of d_{62}-DPPC/GO monolayer. With this purpose, we compare the results obtained for the two surface pressures studied. As can be seen in Table 1, the fraction

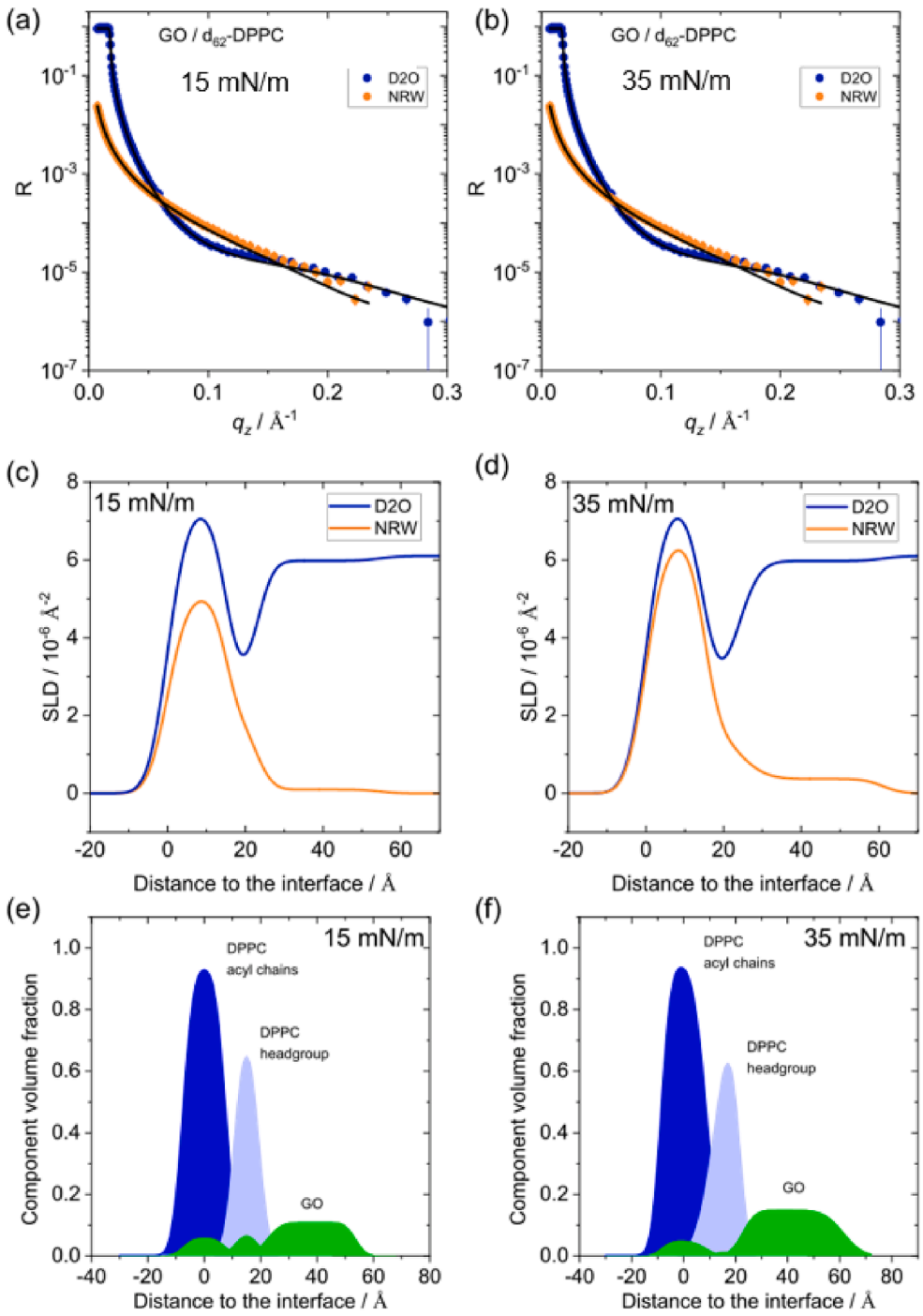

Fig. 4. Neutron Reflectometry experimental data of d_{62}-DPPC monolayers deposited on GO solutions. Experimental (symbols) and simulated (lines) profiles are plotted versus q_z at the surface pressure values of 15 mN/m (a) and 35 mN/m (b). SLD profiles for monolayers at 15 mN/m (c) and 35 mN/m (d). Variation of the volume fractions of different components with the distance normal to the interface for monolayers at: (e) 15 and (f) 35 mN/m.

of GO in the acyl chains of the deuterated phospholipid molecules layer slightly decreases as the surface pressure increases, while it remains constant in the head groups region and increases from 11 % to 15 % in the aqueous GO region. These results point to a displacement of GO sheets from the acyl chains region to the aqueous GO subphase when the surface pressure increases, although it is less marked that the displacement observed for h-DPPC monolayers. Besides, the thickness value of the aqueous GO region (31–39 nm) for deuterated monolayers is like the value obtained for h-DPPC/GO monolayers.

3.5. Effect of GO on the in-plane structure of DPPC thin films studied by GIXD

From results obtained by XRR and NR it is possible to conclude that the GO sheets are distributed not uniformly in the different regions of the monolayer. Besides, the distribution depends on the surface pressure, that means, on the packing of the phospholipid molecules in the monolayer. Therefore, to have a complete description of the structure of DPPC/GO monolayers, we examine the effect of GO insertion on the packing of the h-DPPC monolayers. With this purpose, grazing incidence X-ray diffraction profiles were recorded using synchrotron radiation. We

have selected this technique because X-rays at a grazing angle penetrate deeply, on the order of tens of angstroms, into the air–water interface, making it a very sensitive technique to provide information at the molecular scale of in-plane aliphatic chains packing, the dimensions and tilt of the unit cell and the coherence length, length over which the aliphatic layer diffracts [57]. Our experiments did not show diffraction from the head groups of phospholipid molecules and no higher order diffraction peaks were detected.

Fig. 5 **a-d** shows the corresponding GIXD contour plots of the scattered intensity as a function of q_{xy} and q_z for monolayers of h-DPPC on pure water and deposited on the aqueous GO subphase at surface pressure values of 15 and 35 mN/m, respectively. Besides, Fig. 5**e-f** shows the variation of Bragg peaks of h-DPPC monolayers with and without exposure to the GO solution at the surface pressure values studied.

The 2D contour of the bare h-DPPC monolayer at 15 mN/m, Fig. 5**a,** reveals the existence of two peaks, centered at $q_{xy} = 1.34$ Å^{-1} and $q_{xy} = 1.49$ Å^{-1}. These peaks were previously reported for h-DPPC monolayers and indexed as (01)+(10) and (1 $\bar{1}$) crystallographic planes [32,58,59]. Since the degeneracy of (01) and (10) is not broken, these Bragg peaks give rise to a primitive distorted hexagonal unit cell with dimensions of $|a| = |b|$, and γ, in which the acyl chains of the phospholipid are tilted towards their nearest neighbors (NN). From the inter planar distances, $d_{01} = 4.66$ Å and $d_{11} = 4.24$ Å, the unit cell parameters $|a| = |b| = 5.07$ Å and $\gamma = 113$ ° were calculated. From these parameters an area per molecule, APM, of 47.3 Å^2 was found. Finally, the coherence length along the two crystallographic directions were 40.4 Å and 210 Å, respectively. All these values are in excellent agreement with data in the literature for h-DPPC monolayers [32,60–62].

When the surface pressure increases until 35 mN/m, Fig. 5**c** the peak centered at $q_{xy} = 1.49$ Å^{-1} remains at the same position, while the peak at $q_{xy} = 1.34$ Å^{-1} is shifted toward a higher q_{xy} value and merged with the former peak, being observed as a shoulder at ~ 1.39 Å^{-1}. The shift toward higher q_{xy} observed when the surface pressure increases was previously reported for other systems [61] and is due to the increase of the molecular packing of the aliphatic chains after the monolayer compression.

When GO is incorporated to h-DPPC monolayers, we can see a sequence of GIXD data on a background of much higher intensity, Fig. 5b,d. The higher background looks like a powder ring with q_z which might be caused by the scattering from the subphase due to the high roughness of the interface produced by the GO sheets [63]. Accordingly, the effect is more pronounced for monolayers at 15 mN/m than at 35 mN/m since its roughness is higher, see Table 1.

In Fig. 5**e,f** we compare the Bragg peaks of pristine h-DPPC and h-DPPC in contact with GO monolayers at the two surface pressure studied. As can be seen in Fig. 5**e**, in the GO/h-DPPC monolayer the peak corresponding to h-DPPC centered at $q_{xy} = 1.49$ Å^{-1} is clearly observed, while the peak at $q_{xy} = 1.34$ Å^{-1} appears as a shoulder due to the presence of a new peak at 1.39 Å^{-1}. It is interesting to consider that the position of the Bragg peaks of h-DPPC corresponding to GO/h-DPPC and pristine h-DPPC monolayers are quite similar. This fact indicates that the insertion of GO sheets into the lipid chains does not modify the unit cell of h-DPPC. Another new peak centered at $q_{xy} = 1.52$ Å^{-1} appears. To assign the two new peaks, we consider results obtained for GO adsorbed at the air/water previously reported [63]. These results proved that GO sheets at the water interface give rise to Bragg peaks centered at $q_{xy} = 1.45$ Å^{-1} and 1.497 Å^{-1}, produced by the coexistence of two different diffracting structures, one structure parallel to the plane of the interface, $q_{xy} = 1.497$ Å^{-1}, and another, $q_{xy} = 1.45$ Å^{-1}, assigned to in-plane organization of the GO sheets. The existence of the GO Bragg peaks in the GIXD profile of GO/h-DPPC monolayer at 15 mN/m confirms the insertion of GO sheets in two different regions of the h-DPPC monolayer, the aliphatic chain region, in plane GO structure, and the head groups region, parallel structure. These results are consistent with the information obtained from NR and XRR measurements, although, in the case of GIXD measurements it was not possible to obtain information of the GO layer in the aqueous subphase adjacent to the interface, 3L layer, since GIXD radiation cannot penetrate this layer.

The Bragg peaks of GO/h-DPPC monolayers at 35 mN/m, Fig. 5**f**, show the peaks characteristic of pristine h-DPPC monolayer at 35 mN/m centered at 1.39 and 1.49 Å^{-1}, respectively. The positions of these peaks are the same of the pristine h-DPPC monolayer, indicating that the insertion of GO in the h-DPPC monolayer does not modify the unit cell of h-DPPC. The Bragg peak at 1.51 Å^{-1} assigned to GO parallel to the interface is the most intense Bragg peak, see Fig. 5**f,** and its relative intensity is much higher than that for GO/h-DPPC monolayer at 15 mN/m. Since this peak is assigned to GO sheets parallel to the interface, this behavior indicates that the percentage of GO sheets bound to the head groups of the phospholipid increases as the surface pressure of the monolayer. This result is in excellent agreement to that obtained from reflectometry measurements reported in Fig. 3c and 3d. Finally, the Bragg peak corresponding to GO in plane organization cannot be distinguished in Fig. 5**f,** since it appears at the same position of the Bragg peak of DPPC at 35 mN/m and cannot be separated of it.

4. Conclusions

In the current work using advanced X-Ray and neutron synchrotron techniques, we have modeled, for the first time, the structure of mixed monolayers of GO and the phospholipid DPPC at two different surface pressures values. We used a two-layers model, consisting of aliphatic chains and head groups regions, to interpret the bare DPPC monolayers and a three-layers model, aliphatic chains, head groups and GO in the aqueous subphase regions, for GO/DPPC mixed monolayers. Our results demonstrated that GO sheets are in the three regions, and when the surface pressure increases, the percentage of GO flakes at the aliphatic chains decreases since they are displaced to both, the head groups and the aqueous subphase regions. Comparison between the results obtained for hydrogenated and deuterated aliphatic chains of the phospholipids allows us to demonstrate the interactions between GO and DPPC is due to electrostatic attractions between the positively charged choline groups of DPPC and the carboxylic groups at the edges of GO, and CH–π interactions between the aromatic domains of GO and the aliphatic chains of phospholipid molecules. Our GIXD results also revealed that the insertion of GO sheets in the aliphatic chains region of the DPCC monolayer does not modify the unit cell of DPPC.

We expect that these new insights will help in the design of biosensors or drug carriers with GO as component. Besides, our results unequivocally show the insertion of GO sheets into the aliphatic chains of DPPC; therefore, since in vivo studies conclude that the retention of GO on the lung surfactant film destroys its structure and modifies its biophysical properties, our results point to a potential toxicity of GO sheets. Future work related with the effect of size and surface charge of GO sheets on the insertion of GO in the pure DPPC monolayer and in mixed DPPC monolayers constituted by biological molecules present in the lung surfactant becomes necessary.

CRediT authorship contribution statement

M. Dolores Merchán: Investigation, Writing – review & editing. **Nisha Pawar:** Investigation. **Andreas Santamaria:** Investigation. **Rosalía Sánchez-Fernández:** Investigation. **Oleg Konovalov:** Investigation. **Armando Maestro:** Conceptualization, Investigation, Funding acquisition, Writing – original draft, Writing – review & editing. **M. Mercedes Velázquez:** Conceptualization, Investigation, Funding acquisition, Writing – original draft, Writing – review & editing, Supervision.

Declaration of Competing Interest

The authors declare that they have no known competing financial

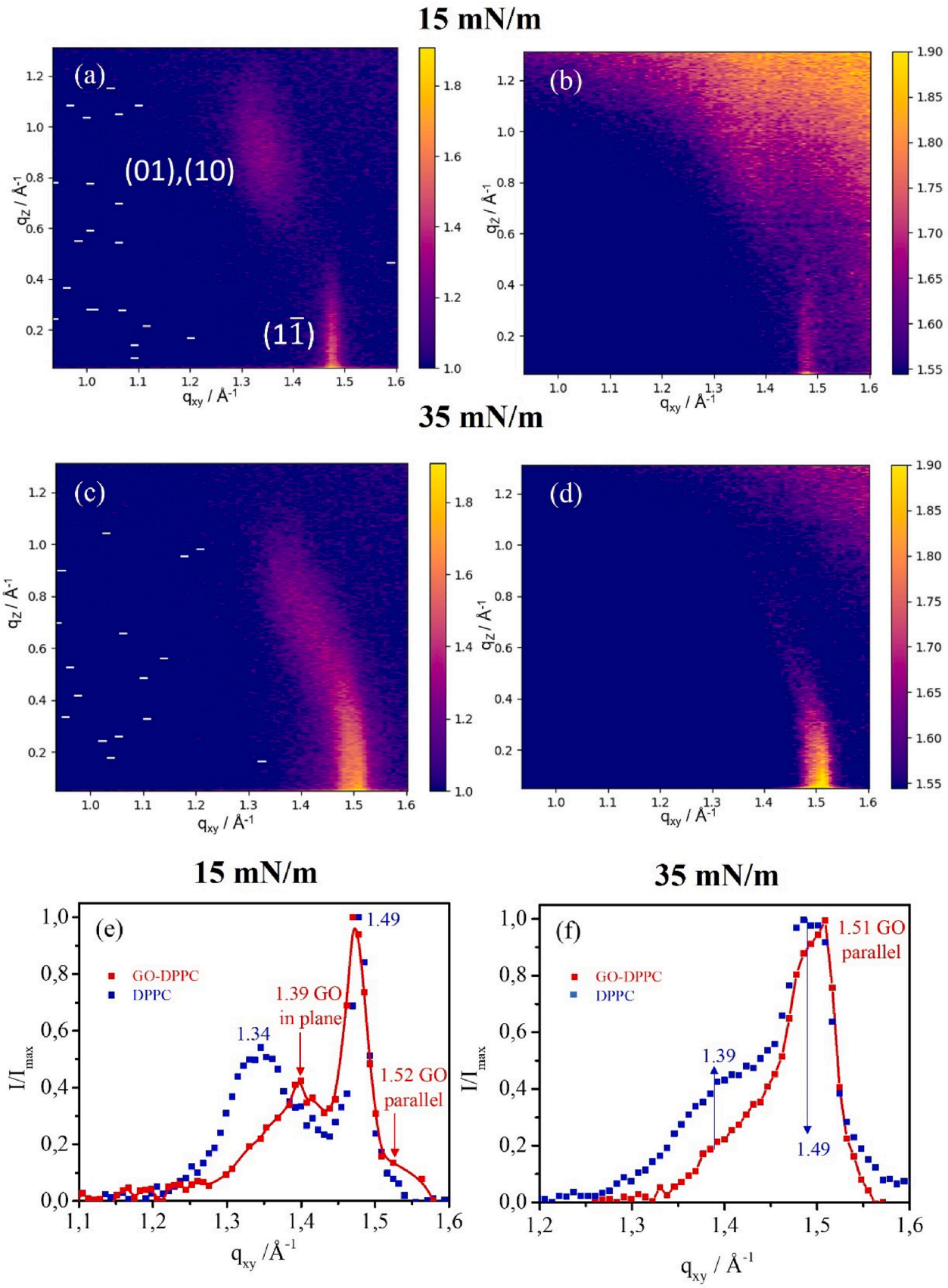

Fig. 5. GIXD intensity contours maps for bare h-DPPC monolayers at the surface pressure values of 15 mN/m (a) and 35 mN/m (b), and for h-DPPC monolayers deposited on the aqueous GO solution at 15 mN/m (c) and 35 mN/m (d). Variation of Bragg peaks with q_{xy} for h-DPPC and GO/h-DPPC at the surface pressure of 15 mN/m (e) and for h-DPPC and GO/h-DPPC at 35 mN/m (f).

interests or personal relationships that could have appeared to influence the work reported in this paper.

Data availability

No data was used for the research described in the article.

Acknowledgment

Authors thank the Institute Laue-Langevin (ILL) for allocation of neutron beam time on FIGARO (DOI: 10.5291/ILL-DATA. 9-13-843) and the European Synchrotron Radiation Facility (ESRF) for provision of synchrotron radiation facilities in beamline ID10 under proposal number LS3159 (DOI:10.15151/ESRF-ES-883953841). We also acknowledge the financial support from European Regional Development Fund, ERDF, Junta de Castilla y León (SA121P20) and MINECO (CTQ2016-78895-R). A.M. acknowledges the financial support from MICINN under grant PID2021-129054NA-I00 and from the IKUR Strategy under the collaboration agreement between Ikerbasque Foundation and Materials Physics Center on behalf of the Department of Education of the Basque Government.

Appendix A. Supplementary material

Supplementary data to this article can be found online at https://doi.org/10.1016/j.jcis.2023.11.022.

References

[1] R.S. Hidalgo, D. López-Díaz, M.M. Velázquez, Graphene Oxide Thin Films: Influence of Chemical Structure and Deposition Methodology, Langmuir 31 (9) (2015) 2697–2705.
[2] D. López-Díaz, M. López Holgado, J.L. García-Fierro, M.M. Velázquez, Evolution of the Raman Spectrum with the Chemical Composition of Graphene Oxide, J. Phys. Chem. C 121 (37) (2017) 20489–20497.
[3] H. He, T. Riedl, A. Lerf, J. Klinowski, Solid-State NMR Studies of the Structure of Graphite Oxide, J. Phys. Chem. 100 (51) (1996) 19954–19958.
[4] A. Lerf, H. He, M. Forster, J. Klinowski, Structure of Graphite Oxide Revisited‖, J. Phys. Chem. B 102 (23) (1998) 4477–4482.
[5] J.P. Rourke, P.A. Pandey, J.J. Moore, M. Bates, I.A. Kinloch, R.J. Young, N. R. Wilson, The Real Graphene Oxide Revealed: Stripping the Oxidative Debris from the Graphene-like Sheets, Angew. Chem. Int. Ed. 50 (14) (2011) 3173–3177.
[6] S.P.D. Helen, R. Thomas, W.E. Woodruff, C. Vallés, R.J. Young, I.A. Kinloch, G. W. Morley, J.V. Hanna, N.R. Wilson, J.P. Rourke, Deoxygenation of Graphene Oxide: Reduction or Cleaning? Chem. Mater. 25 (18) (2013) 3580–3588.
[7] D. López-Díaz, M.D. Merchán, M.M. Velázquez, A. Maestro, Understanding the Role of Oxidative Debris on the Structure of Graphene Oxide Films at the Air-Water Interface: A Neutron Reflectivity Study, ACS Appl. Mater. Interfaces 12 (2020) 25453–25463.
[8] D. López-Diaz, M.D. Merchán, M.M. Velázquez, The behavior of graphene oxide trapped at the air water interface, Adv. Colloid Interface Sci. 286 (2020), 102312.
[9] D. López-Díaz, M.M. Velázquez, S. Blanco de La Torre, A. Pérez-Pisonero, R. Trujillano, J.L.G. Fierro, S. Claramunt, A. Cirera, The Role of Oxidative Debris on Graphene Oxide Films, ChemPhysChem 14 (17) (2013) 4002–4009.
[10] S.K. Saha, S. Bhaumik, T. Maji, T.K. Mandal, A.J. Pal, Solution-processed reduced graphene oxide in light-emitting diodes and photovoltaic devices with the same pair of active materials, RSC Adv. 4 (67) (2014) 35493–35499.
[11] G. Eda, M. Chhowalla, Chemically Derived Graphene Oxide: Towards Large-Area Thin-Film Electronics and Optoelectronics, Adv. Mater. 22 (22) (2010) 2392–2415.
[12] D. Mendez-Gonzalez, O.G. Calderón, S. Melle, J. González-Izquierdo, L. Bañares, D. López-Díaz, M.M. Velázquez, E. López-Cabarcos, J. Rubio-Retama, M. Laurenti, Contribution of resonance energy transfer to the luminescence quenching of upconversion nanoparticles with graphene oxide, J. Colloid Interface Sci. 575 (2020) 119–129.
[13] G.K. Yogesh, E.P. Shuaib, P. Roopmani, M.B. Gumpu, U.M. Krishnan, D. Sastikumar, Synthesis, characterization and bioimaging application of laser-ablated graphene-oxide nanoparticles (nGOs), Diam. Relat. Mater. 104 (2020), 107733.
[14] J. Liu, L. Cui, D. Losic, Graphene and graphene oxide as new nanocarriers for drug delivery applications, Acta Biomater. 9 (12) (2013) 9243–9257.
[15] Y. Wei, F. Zhou, D. Zhang, Q. Chen, D. Xing, A graphene oxide based smart drug delivery system for tumor mitochondria-targeting photodynamic therapy, Nanoscale 8 (6) (2016) 3530–3538.
[16] F. Grilli, P. Hajimohammadi Gohari, S. Zou, Characteristics of Graphene Oxide for Gene Transfection and Controlled Release in Breast Cancer Cells, Int. J. Mol. Sci. 23 (12) (2022).
[17] H. Watson, Biological membranes, Essays Biochem. 59 (2015) 43–69.
[18] R. Muñoz-López, E. Guzmán, M.M. Velázquez, L. Fernández-Peña, M.D. Merchán, A. Maestro, F. Ortega, R.G. Rubio, Influence of Carbon Nanosheets on the Behavior of 1,2-Dipalmitoyl-sn-glycerol-3-phosphocholine Langmuir Monolayers, Processes 8 (1) (2020) 94.
[19] K. Donaldson, A. Seaton, A short history of the toxicology of inhaled particles, Part. Fibre Toxicol. 9 (1) (2012) 13.
[20] C.M. Beddoes, C.P. Case, W.H. Briscoe, Understanding nanoparticle cellular entry: A physicochemical perspective, Adv. Colloid Interface Sci. 218 (2015) 48–68.
[21] A. Rhazouani, H. Gamrani, M. El Achaby, K. Aziz, L. Gebrati, M.S. Uddin, F. Aziz, Synthesis and Toxicity of Graphene Oxide Nanoparticles: A Literature Review of In Vitro and In Vivo Studies, Biomed Res. Int. 2021 (2021) 5518999.
[22] L. Ou, B. Song, H. Liang, J. Liu, X. Feng, B. Deng, T. Sun, L. Shao, Toxicity of graphene-family nanoparticles: a general review of the origins and mechanisms, Part. Fibre Toxicol. 13 (1) (2016) 57.
[23] B. Li, J. Yang, Q. Huang, Y. Zhang, C. Peng, Y. Zhang, Y. He, J. Shi, W. Li, J. Hu, C. Fan, Biodistribution and pulmonary toxicity of intratracheally instilled graphene oxide in mice, NPG Asia Mater. 5 (4) (2013) e44–e.
[24] Q. Hu, B. Jiao, X. Shi, R.P. Valle, Y.Y. Zuo, G. Hu, Effects of graphene oxide nanosheets on the ultrastructure and biophysical properties of the pulmonary surfactant film, Nanoscale 7 (43) (2015) 18025–18029.
[25] F. Wang, J. Liu, H. Zeng, Interactions of particulate matter and pulmonary surfactant: Implications for human health, Adv. Colloid Interface Sci. 284 (2020), 102244.
[26] E. Guzmán, E. Santini, Lung surfactant-particles at fluid interfaces for toxicity assessments, Curr. Opin. Colloid Interface Sci. 39 (2019) 24–39.
[27] E. Lopez-Rodriguez, J. Pérez-Gil, Structure-function relationships in pulmonary surfactant membranes: from biophysics to therapy, Biochim Biophys Acta 1838 (6) (2014) 1568–1585.
[28] T.R. Sosnowski, P. Kubski, K. Wojciechowski, New experimental model of pulmonary surfactant for biophysical studies, Colloids Surf. A Physicochem. Eng. Asp 519 (2017) 27–33.
[29] S. Li, A.J. Stein, A. Kruger, R.M. Leblanc, Head Groups of Lipids Govern the Interaction and Orientation between Graphene Oxide and Lipids, J. Phys. Chem. C 117 (31) (2013) 16150–16158.
[30] R. Frost, G.E. Jönsson, D. Chakarov, S. Svedhem, B. Kasemo, Graphene Oxide and Lipid Membranes: Interactions and Nanocomposite Structures, Nano Lett. 12 (7) (2012) 3356–3362.
[31] L. Wu, L. Zeng, X. Jiang, Revealing the Nature of Interaction between Graphene Oxide and Lipid Membrane by Surface-Enhanced Infrared Absorption Spectroscopy, J. Am. Chem. Soc. 137 (32) (2015) 10052–10055.
[32] P. Mandal, R.P. Giri, B.M. Murphy, S.K. Ghosh, Self-Assembly of Graphene Oxide Nanoflakes in a Lipid Monolayer at the Air-Water Interface, ACS Appl. Mater. Interfaces 13 (48) (2021) 57023–57035.
[33] P. Mandal, G. Bhattacharya, A. Bhattacharyya, S.S. Roy, S.K. Ghosh, Unravelling the structural changes of phospholipid membranes in presence of graphene oxide, Appl. Surf. Sci. 539 (2021), 148252.
[34] J. Chen, G. Zhou, L. Chen, Y. Wang, X. Wang, S. Zeng, Interaction of Graphene and its Oxide with Lipid Membrane: A Molecular Dynamics Simulation Study, J. Phys. Chem. C 120 (11) (2016) 6225–6231.
[35] Y. Tu, M. Lv, P. Xiu, T. Huynh, M. Zhang, M. Castelli, Z. Liu, Q. Huang, C. Fan, H. Fang, R. Zhou, Destructive extraction of phospholipids from Escherichia coli membranes by graphene nanosheets, Nat. Nanotechnol. 8 (8) (2013) 594–601.
[36] L. Braun, M. Uhlig, R. von Klitzing, R.A. Campbell, Polymers and surfactants at fluid interfaces studied with specular neutron reflectometry, Adv. Colloid Interface Sci. 247 (2017) 130–148.
[37] A. Maestro, P. Gutfreund, In situ determination of the structure and composition of Langmuir monolayers at the air/water interface by neutron and X-ray reflectivity and ellipsometry, Adv. Colloid Interface Sci. 293 (2021), 102434.
[38] M. Delcea, C.A. Helm, X-ray and Neutron Reflectometry of Thin Films at Liquid Interfaces, Langmuir 35 (26) (2019) 8519–8530.
[39] A.G.E. Jean Daillant, X-ray and Neutron Reflectivity: Principles and Applications, Springer, Berlin, Heidelberg, 2009.
[40] V.M. Kaganer, H. Möhwald, P. Dutta, Structure and phase transitions in Langmuir monolayers, Rev. Mod. Phys. 71 (3) (1999) 779–819.
[41] G. Brezesinski, H. Möhwald, Langmuir monolayers to study interactions at model membrane surfaces, Adv. Colloid Interface Sci. 100–102 (2003) 563–584.
[42] E. Madrid, S.L. Horswell, Effect of Deuteration on Phase Behavior of Supported Phospholipid Bilayers: A Spectroelectrochemical Study, Langmuir 31 (45) (2015) 12544–12551.
[43] M.V. Smoluchowski, Handbuch der Elektrizität und des Magnetismus, Graetz, Leipzig, 1921.
[44] R.A. Campbell, H.P. Wacklin, I. Sutton, R. Cubitt, G. Fragneto, FIGARO: The new horizontal neutron reflectometer at the ILL, Eur. Phys. J. Plus 126 (11) (2011) 107.
[45] R.A. Campbell, Recent advances in resolving kinetic and dynamic processes at the air/water interface using specular neutron reflectometry, Curr. Opin. Colloid Interface Sci. 37 (2018) 49–60.
[46] P. Gutfreund, T. Saerbeck, M.A. Gonzalez, E. Pellegrini, M. Laver, C. Dewhurst, R. Cubitt, Towards generalized data reduction on a chopper-based time-of-flight neutron reflectometerThis article will form part of a virtual special issue on advanced neutron scattering instrumentation, marking the 50th anniversary of the journal, J. Appl. Cryst. 51 (3) (2018) 606–615.
[47] Y. Gerelli, Aurore: new software for neutron reflectivity data analysis. Corrigendum, J. Appl. Cryst. 49 (2) (2016) 712.
[48] A.R.J. Nelson, S.W. Prescott, refnx: neutron and X-ray reflectometry analysis in Python, J. Appl. Cryst. 52 (1) (2019) 193–200.

[49] K. Kjaer, J. Als-Nielsen, C.A. Helm, L.A. Laxhuber, H. Möhwald, Ordering in Lipid Monolayers Studied by Synchrotron X-Ray Diffraction and Fluorescence Microscopy, Phys. Rev. Lett. 58 (21) (1987) 2224–2227.
[50] C.A. Helm, H. Möhwald, K. Kjær, J. Als-Nielsen, Phospholipid Monolayer Density Distribution Perpendicular to the Water Surface. A Synchrotron X-Ray Reflectivity Study, Europhys. Lett. 4 (6) (1987) 697.
[51] M. Schalke, M. Lösche, Structural models of lipid surface monolayers from X-ray and neutron reflectivity measurements, Adv. Colloid Interface Sci. 88 (1) (2000) 243–274.
[52] L.G. Parratt, Surface Studies of Solids by Total Reflection of X-Rays, Phys. Rev. 95 (2) (1954) 359–369.
[53] R.A. Campbell, Y. Saaka, Y. Shao, Y. Gerelli, R. Cubitt, E. Nazaruk, D. Matyszewska, M.J. Lawrence, Structure of surfactant and phospholipid monolayers at the air/water interface modeled from neutron reflectivity data, J. Colloid Interface Sci. 531 (2018) 98–108.
[54] J.F. Nagle, S. Tristram-Nagle, Structure of lipid bilayers, Biochim. Biophys. Acta (BBA) – Rev. Biomembr. 1469 (3) (2000) 159–195.
[55] M. Nishio, The CH/π hydrogen bond in chemistry. Conformation, supramolecules, optical resolution and interactions involving carbohydrates, Phys. Chem. Chem. Phys. 13(31) (2011) 13873-13900.
[56] J. Ribas, E. Cubero, F.J. Luque, M. Orozco, Theoretical Study of Alkyl-π and Aryl-π Interactions. Reconciling Theory and Experiment, J. Organic Chem. 67 (20) (2002) 7057–7065.
[57] J. Als-Nielsen, D. Jacquemain, K. Kjaer, F. Leveiller, M. Lahav, L. Leiserowitz, Principles and applications of grazing incidence X-ray and neutron scattering from ordered molecular monolayers at the air-water interface, Phys. Rep. 246 (5) (1994) 251–313.
[58] C.E. Miller, D.D. Busath, B. Strongin, J. Majewski, Integration of Ganglioside GT1b Receptor into DPPE and DPPC Phospholipid Monolayers: An X-Ray Reflectivity and Grazing-Incidence Diffraction Study, Biophys. J . 95 (7) (2008) 3278–3286.
[59] J. Majewski, B. Stec, X-ray scattering studies of model lipid membrane interacting with purothionin provide support for a previously proposed mechanism of membrane lysis, Eur. Biophys. J. 39 (8) (2010) 1155–1165.
[60] F. Neville, Y. Ishitsuka, C.S. Hodges, O. Konovalov, A.J. Waring, R. Lehrer, K.Y. C. Lee, D. Gidalevitz, Protegrin interaction with lipid monolayers: grazing incidence X-ray diffraction and X-ray reflectivity study, Soft Matter 4 (8) (2008) 1665–1674.
[61] E.B. Watkins, C.E. Miller, W.P. Liao, T.L. Kuhl, Equilibrium or quenched: fundamental differences between lipid monolayers, supported bilayers, and membranes, ACS Nano 8 (4) (2014) 3181–3191.
[62] K. Andreev, The Structural Role of Gangliosides: Insights from X-ray Scattering on Model Membranes, Curr. Med. Chem. 27 (38) (2020) 6548–6570.
[63] N. Bonatout, F. Muller, P. Fontaine, I. Gascon, O. Konovalov, M. Goldmann, How exfoliated graphene oxide nanosheets organize at the water interface: evidence for a spontaneous bilayer self-assembly, Nanoscale 9 (34) (2017) 12543–12548.